Surface Representations of Two- and Three-Dimensional Fluid Flow Topology

J. L. Helman
Department of Applied Physics

Lambertus Hesselink
Departments of Aeronautics/Astronautics and Electrical Engineering

Stanford University
Stanford, CA 94305-4035

Abstract

We discuss our work using critical point analysis to generate representations of the vector field topology of numerical flow data sets. Critical points are located and characterized in a two-dimensional domain, which may be either a two-dimensional flow field or the tangential velocity field near a three-dimensional body. Tangent curves are then integrated out along the principal directions of certain classes of critical points. The points and curves are linked to form a skeleton representing the two-dimensional vector field topology.

When generated from the tangential velocity field near a body in a three-dimensional flow, the skeleton includes the critical points and curves which provide a basis for analyzing the three-dimensional structure of the flow separation. The points along the separation curves in the skeleton are used to start tangent curve integrations to generate surfaces representing the topology of the associated flow separations.

1. Introduction

When computer graphics is introduced to a field of study, the visualization techniques to emerge first are the ones which most closely resemble the "pictures" already in use and familiar to those in the field. To the researcher, who having seen thousands of them, has learned to interpret them, such images may be more useful than a new representation which actually contains more information. What X-ray images are to radiologists, and multiple needle strip chards are to seismologists, so oil streak patterns and smoke visualizations are to fluid dynamicists. The capabilities of the first generation of numeric flow visualization packages, such as PLOT3D[1] reflect this approach. To visualize oil film patterns on the surface of a body in a flow, the tangential flow near the surface is integrated to generate curves on the body wall. To duplicate smoke visualizations (albeit without mass and diffusion), massless particles can be integrated through the flow to generate streamlines.

In many fields, computer aided visualization of scientific data is moving beyond previous experimental visualizations both in the form of the graphic representations and in the level of abstraction or scientific data interpretation used to produce the pictures. Direct visualization methods in which thousands of points, vectors or curves are displayed are inadequate for visualizing many complex data sets, and manually chosing a smaller set of elements for direct display is usually both time consuming and error prone.

The importance of topology in understanding fluid dynamics[2][3][4] combined with the difficulty of extracting topological information with existing tools has motivated our efforts. This paper describes some of the methods we have developed to automate the analysis and display of vector field topology in general and flow topology in particular. We fist discuss the two-dimensional case, since it provides the basis for our examination of topology in three-dimensional separated flows.

2. Two-Dimensional Vector Field Topology

Topological concepts are very powerful because given the critical points in a vector field and the tangent curves or surfaces connecting them, one can infer the shape of other tangent curves and hence to some extent the structure of the entire vector field.

Flow topology can be thought of in terms of surfaces in three-dimensional flows or curves in two-dimensional flows which divide the flow into separate regions. Two sets of surfaces or lines are of particular interest [5]. The first set are those along which the flow close to the

CH2913-2/90/0000/0006/$01.00 – 1990 IEEE

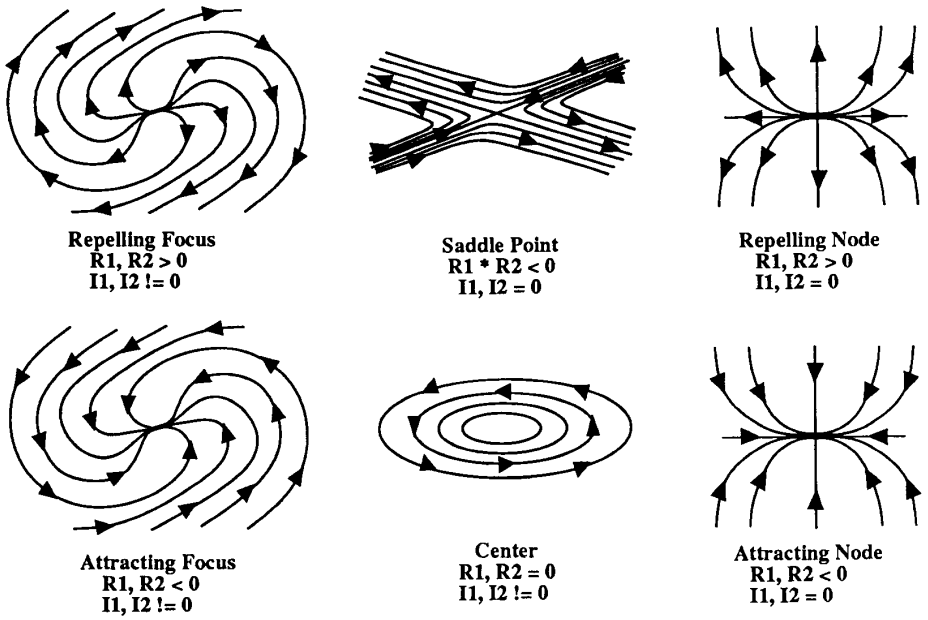

Figure 1: Classification criteria for critical points. R1 and R2 denote the real parts of the eigenvalues of the Jacobian, I1 and I2 the imaginary parts.

wall of a body attaches to or separates from that wall, i.e., those tangent curves which actually end on the wall rather than moving along the surface. The second set are those surfaces where tangent curves which start arbitrarily close to each other can end up in substantially different regions. This second group of curves are related to critical points. For example, tangent curves on either side of a curve that goes directly into a saddle point are diverted by the saddle point to very different regions.

2.1. Critical Points. Critical points are those points at which the magnitude of the vector vanishes. These points may be characterized according to the behavior of nearby tangent curves. The set of tangent curves which end on critical points are of special interest because they define the behavior of the vector field in the neighborhood of the point. A particular set of these curves can be used to define a skeleton which characterizes the global behavior of all other tangent curves in the vector field.

To first order approximation, a critical point can be classified according to the eigenvalues of the Jacobian matrix of the vector (u, v) with respect to position at the critical point $(x0, y0)$:

$$\left.\frac{\partial(u,v)}{\partial(x,y)}\right|_{x0,y0} = \left.\begin{bmatrix} \frac{\partial u}{\partial x} & \frac{\partial u}{\partial y} \\ \frac{\partial v}{\partial x} & \frac{\partial v}{\partial y} \end{bmatrix}\right|_{x0,y0} \quad (1)$$

Figure 1 shows how the eigenvalues classify a critical point as an *attracting node*, a *repelling node*, an *attracting focus*, a *repelling focus*, a *center* or a *saddle*. This can be understood by observing that a positive or negative real part of an eigenvalue indicates an attracting or repelling nature, respectively. The imaginary part denotes circulation about the point. Among these points, the saddle points are distinct in that there are only four tangent curves which actually end at the point itself. At the saddle point, these curves are tangent to the two eigenvectors of the Jacobian matrix, which are the separatrices of the saddle point. The outgoing and incoming separatrices are parallel to the eigenvectors with positive and negative eigenvalues, respectively.

In addition to these 2-D critical points, certain points on the walls of objects or bodies in a fluid flow can be important. On walls where the velocity is constrained to be zero (no slip boundary in fluid dynamics), there may occur certain points, referred to as, *attachment nodes* or *detachment nodes* at which a tangent curve impinging on the surface terminates on the surface, rather than being deflected by the tangential velocity.

The saddle points, attachment and detachment nodes differ from the other points in two regards. First, there are only a finite number of tangent curves (two for saddles, and one for the attachment/detachment nodes) which end on the point itself. Second, the curves adjacent to these particular curves diverge at the critical point, which makes these curves significant to understanding the global behavior of other tangent curves. These curves connect the various critical points into a skeleton which represents the global topology of the two-

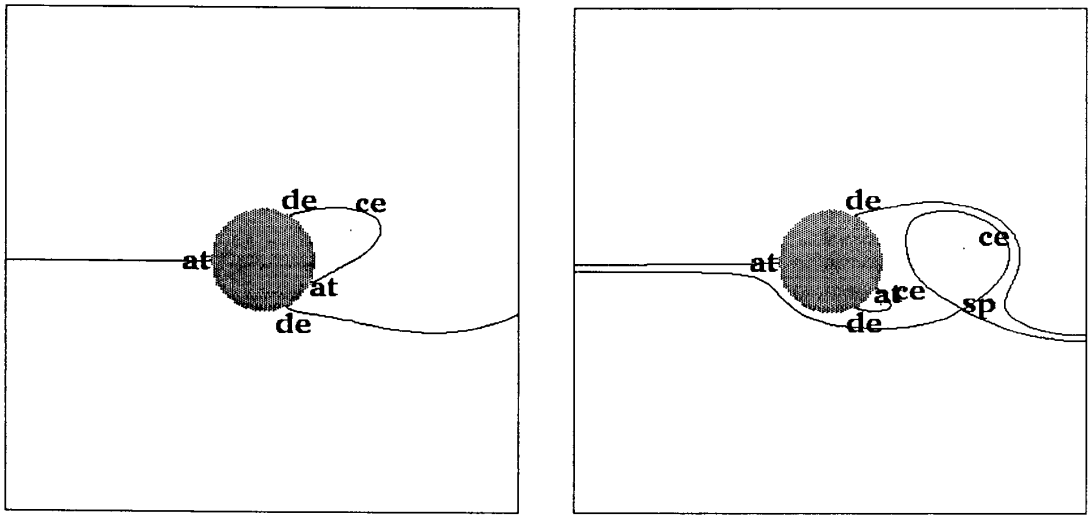

Figure 2: Topology schematics for two time steps in the computed flow around a circular cylinder.

dimensional vector field, thus providing a very effective simplification for complex fields. The details of the analysis and generation of the representations are discussed elsewhere[6].

Figure 2 shows the topology skeletons generated for two time steps in a computed two-dimensional flow around a circular cylinder[7]. The flow is incident from the left with one instantaneous streamline ending directly on the front of the cylinder. All instantaneous streamlines starting above that curve are deflected over the top of the cylinder, and those starting below it are deflected beneath it. Vortex shedding occurs behind the cylinder as indicated by the detachment-attachment "bubble" in the first skeleton developing into a paired saddle and center in the second.

2.2. Two-Dimensional Time-Dependent Flows. When a two-dimensional vector field depends on time or another parameter, the instantaneous topology skeletons can be linked together to denote the time evolution of the flow. The adjacent skeletons are joined by linking their corresponding points and tangent curves. This provides a representation of the time development of the topologies which can be used to examine the formation of structures and to locate topological transitions.

The internal graph representation of the skeleton is used to identify topological transitions. Corresponding points and curves are identified using the saddle, detachment and attachment points as a basis. For each of these points the corresponding principal curves are linked and the algorithm is applied recursively to the end points to ensure consistency.

After the instantaneous slices have been linked together, the set of stacked topological representations can be displayed as a set of surfaces with the third dimension corresponding to time. The surfaces are created by tesselating strips between corresponding tangent curves in adjacent slices of the representation. A strip can be drawn only when the start and end points of the curve in one slice are linked to the start and end points of the curve in the next slice. If a topological transition has occurred, the surface between the time steps cannot be drawn without knowledge of the intermediate topology. Currently, these surfaces are omitted from the display.

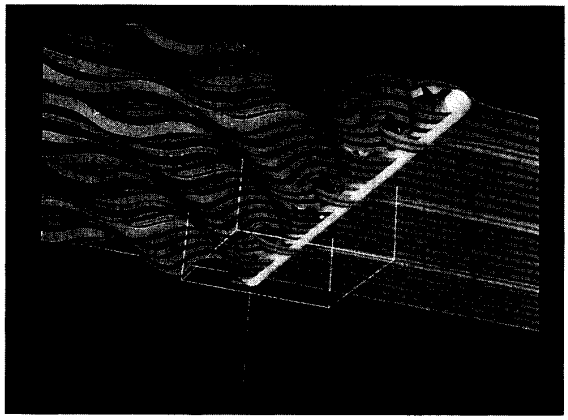

Figure 3: Topological surfaces depicting the time evolution of the computed 2-D flow past a circular cylinder. ***(Color Plate 1, page 460)***

Figure 3 shows the surfaces in the periodic flow around a two-dimensional circular cylinder. Time increases from back to front along the cylinder. The dis-

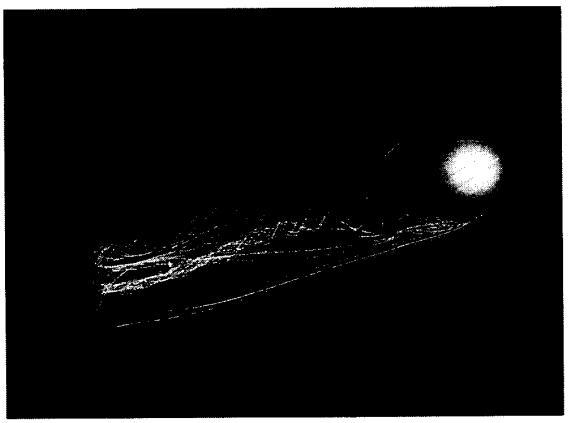

Figure 4: Streamlines in the computed flow past a hemisphere cylinder. ***(Color Plate 2, page 460)***

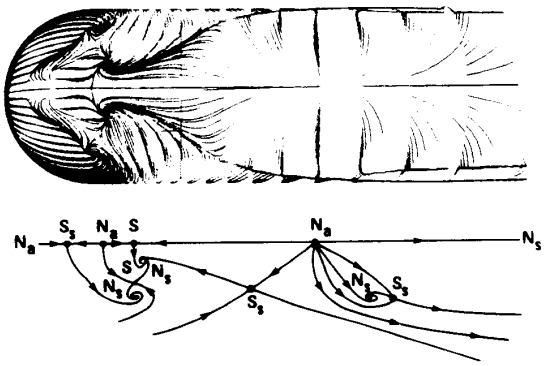

Figure 5: a. Surface particle traces in the computed flow past a hemisphere cylinder. b. Corresponding manually generated schematic interpretation of surface topology. Both from Ying *et al.*[8]

play utilizes several cues to aid visualization. The surfaces are lighted and shaded, and they are colored according to their type. Surfaces corresponding to the incoming separatrix of a saddle point are colored yellow. Those surfaces corresponding to the outgoing direction are colored blue. Surfaces from attachment points are colored orange, and those from detachment points are colored purple. The periodic vortex shedding can be seen in the repeated development and movement downstream of a saddle-center pairs.

3. Topology in Three-Dimensional Separated Flows

The primary purpose of our two-dimensional work was to develop techniques that could be extended to the

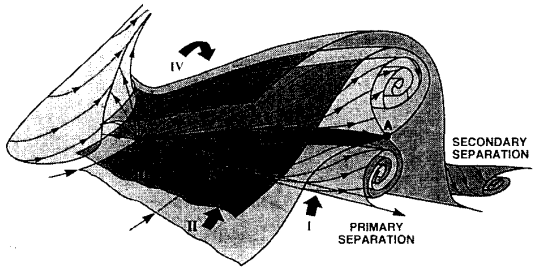

Figure 6: Hand drawn surfaces depicting separation topology for the computed flow past a hemisphere cylinder. From Ying et al.[8] ***(Color Plate 3, page 460)***

study of three-dimensional separated flows. In these flows some stream surfaces near the surface of a body can abruptly move away and "separate" from the wall. The lines at which this occurs are known as "lines of separation." These lines are the three-dimensional extension of the *attachment nodes* and *detachment nodes* used in the two-dimensional analysis. Namely, these are curves on a body wall along which the tangent curves impinging on the body come very close to the surface and end on a critical point on the surface of the body rather than being deflected around it.

Because separation surfaces are often associated with vortices and recirculation zones, determining separation topologies is important both for understanding fundamental fluid dynamics and practical applications in aircraft and jet nozzle design. But extracting topological information from numerical data sets using existing visualization tools is both difficult and time consuming. Typically, a researcher would try to determine the topology and the positions and shapes of the structures by looking at numerically integrated streamlines both in the volume (Figure 4) as well as integrations constrained to the surface (Figure 5a). By manually selecting and refining integration starting points, structures and connections can be discerned. But since topological structures are complex and best portrayed graphically, those structures must then be hand drawn (Figures 5b. and 6) to capture the form of the structures, if not their exact shape, size, and position. Automatic methods of producing these schematic surfaces would not only simplify the work and eliminate manual errors, but most importantly, would accurately preserve and convey the quantitative aspects of the structures.

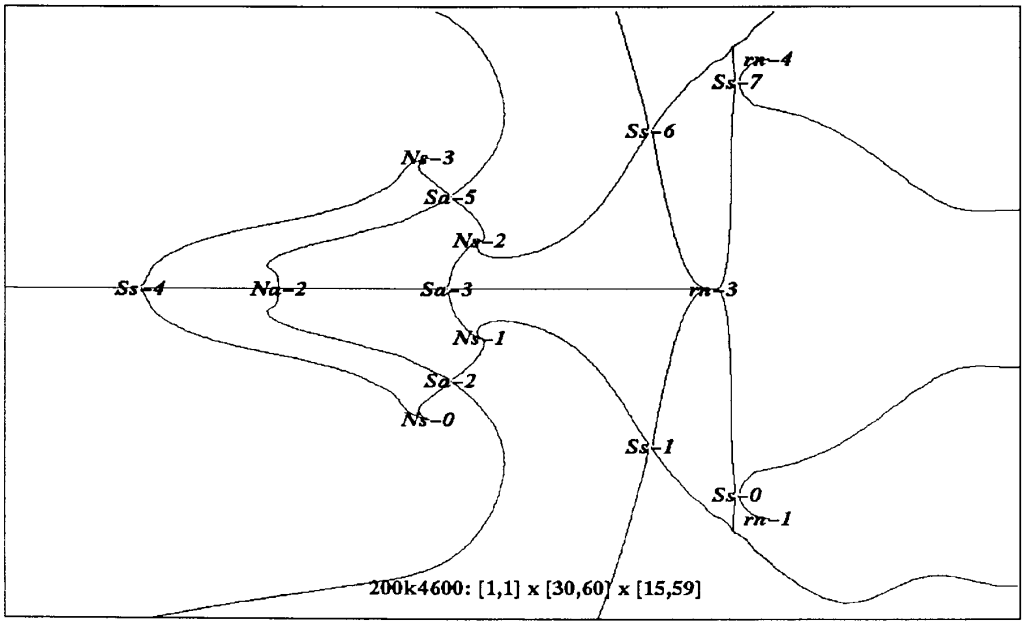

Figure 7: Computer generated skeleton of surface topology corresponding to Figure 5

3.1. Surface Topology. In general, when examining the topology of a flow, the surfaces of bodies in the flow are examined first. In experimental work, this is done by examining the streaks that form in an oil film on the surface of a body in a wind tunnel. In computer simulated flows, similar information can be derived by examining curves integrated along the surface [8] as in Figure 5a to produce topology skeletons like that shown in Figure 5b.

We can automatically generate the surface topology skeleton by applying the two-dimensional algorithm outlined above to the tangential velocity field near the body. Grids in these data sets conform to the shape of the body with one of the grid planes lying on the surface of the body. The velocity on this plane is zero. To analyze the surface topology, we create the two-dimensional vector field which is the projection of the velocities in the grid plane one point away from the surface. If the body is defined by the $k = 0$ grid plane, the new two-dimensional field $(u'(i,j), v'(i,j))$ is computed as the projection of the three-dimensional velocity $(u(i,j,k), v(i,j,k), w(i,j,k))$ into the plane tangent to the body at $(i,j,0)$

Applying the same algorithm which generated the skeletons in Figure 2 to this field produces the surface topology skeleton in Figure 7. Here the critical points have been labeled according to the sign of the normal component. *Ss* denotes a saddle of separation (normal velocity positive), and *Sa* denotes a saddle of attachment (normal velocity negative).

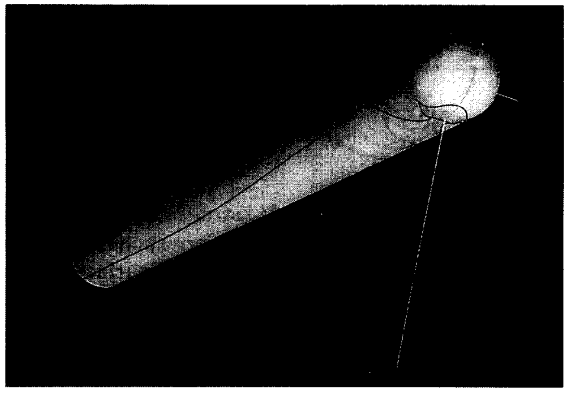

Figure 8: Surface topology skeleton shown on the body surface. ***(Color Plate 4, page 460)***

The positions and connections hypothesized by Ying et al. (Figure 5b) correspond well with this skeleton. The scale distortions are due to the use of grid index coordinates in Figure 7 rather than unrolled physical coordinates. Figure 8 shows these curves projected onto the surface of the hemisphere cylinder body. The curves incoming to and outgoing from saddle points are colored yellow and blue, respectively.

The one minor difference between these figures is the position of the point *rn-1* (and it's symmetry reflection

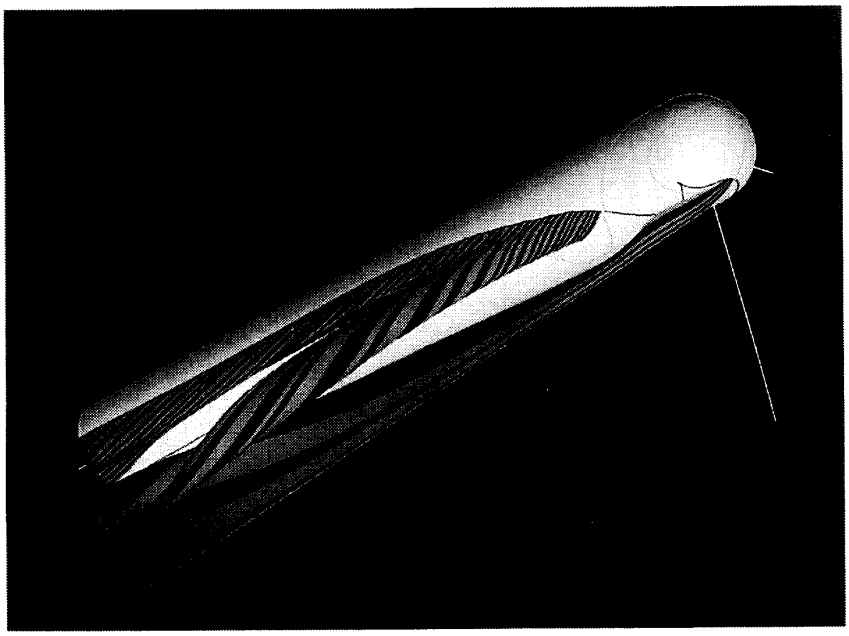

Figure 9: Computer generated surfaces depicting separation topology.
(Color Plate 5, page 460)

rn-4). The difference can be attributed to the coarse resolution of the grid in this region. The data set contains the topology shown in Figure 7, but the physically correct solution has the topology shown in Figure 5.

3.2. Three-Dimensional Separation Structures. As shown in Figure 6, the saddles of separation on the surface generate complex surfaces of separation. These points, which are saddles in the tangent plane are repelling nodes in the plane normal to the surface and parallel to the outgoing separatrix (blue line) of the saddle point. The stream surface generated by this repelling node is the surface of separation. This can be seen in the surface generated by the saddles of separation labeled S_s in Figure 6. In principal, this entire stream surface could be generated by starting curve integrations in this plane in the neighborhood of the point. But note the manner in which the curves move away from the surface along separation curves labeled I and III downstream from the saddles. The normal velocity along these lines of separation on the body is sufficiently large that given reasonable grid spacings, it is impossible to start integrations close enough to the surface so that they will remain near the surface downstream. Thus in practice, the surfaces of separation cannot be generated solely from integrations in the neighborhood of the saddles of separation.

However, from our integrations of the two-dimensional tangential field, for each saddle, we know the corresponding separation curves on the surface (the blue curves in Figure 8). Since analytically, as the starting point gets arbitrarily close to the body, the integrated curve should approach the separation curve, the separation curve can provide starting points for integrating curves into the external flow. The results of integrating stream lines along two separation curves and tesselating them with a surface are shown in Figure 9.

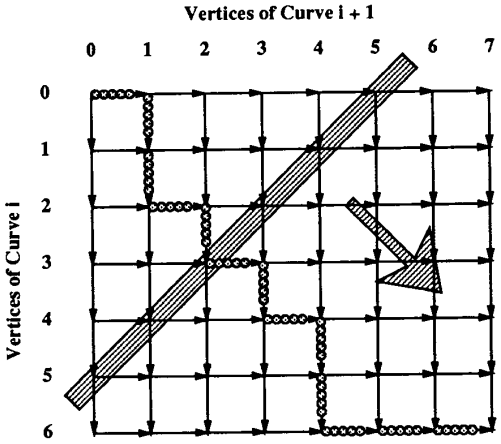

Figure 10: Directed graph used in optimal surface generation. Diagonal box and arrow denote the search order.

3.3. Tesselation. To generate surfaces from adjacent curves, a polygonal tesselation must be defined. In this

Figure 11: Close up of separation surfaces showing divergence of integrated curves.
(Color Plate 6, page 460)

work, we are tiling the surface with a triangular mesh. Given two curves C_1 and C_2 which are defined as a series of line segments connecting the vertices $C_1(i) : 0 < i < n-1$ and $C_2(j) : 0 < j < m-1$ there are $(m+n)!/(m!n!)$ different triangular tesselations of the surface consistent with those line segments! The correct surface would be the one which comes closest to the surface that would be defined by all the other intermediate curves which we did not integrate. We could compute enough of these curves so that their density would exceed the display resolution, but that is impractical.

A simple and computationally expedient method is to assign triangles along the curves matching the fractional distance between 0 and 1 along each curve. This method, however, fares poorly when adjacent curves have slightly different winding counts going into a focus and when curves with inflection points are shifted, e.g. $(x, y, z) = (x, x^3, 0) : -0.5 < x < 0.5$ and $(x, y, z) = (x, x^3 + 1, 1) : -0.4 < x < 0.6$.

A natural surface to chose is one which minimizes the surface area (as a soap bubble does). To do this in a reasonably efficient fashion, we adapted an algorithm developed for tesselating closed contours in parallel cross sections[9] in which each segment between the curves defining the edge of a triangle corresponds to a vertex in a directed graph and each triangle corresponds to an edge in the graph (Figure10. By assigning a cost to each edge in the graph, finding an optimal tesselation is reduced to the problem of finding a least cost path through the graph from the vertex $(0, 0)$ to the vertex (n, m). This can be done quite simply by computing the lowest cost for each vertex along the diagonal $i + j = C$ starting with $C = 1$ and ending with $C = m + n - 2$. At each of these vertices, this requires the computation of the cost of moving from either of two vertices on the previous diagonal (or only one previous vertex when the current vertex is on a border of the graph) to the vertex under consideration on the diagonal, requiring $O(mn)$ operations.

This global optimal path determination is computationally intensive, but we have not found any local heuristic or faster global tesselation method which works as well.

3.4. Refinement and Stability. As can be seen in Figure 9, curves starting from the lines of separation have widely varying spacings as they move downstream. In fact, the curves integrated with starting points along the primary line of separation curl up into two distinct vortices. Since the curve is not known until it is integrated, the curves are created by successive refinement until the end points of the curves are within some specified tolerance. But near the place where the surface "splits" into two vortices, integrated curves exhibit extreme sensitivity to initial conditions (Figure 11). In principal, there is a continuous surface which joins the two. However, the extreme sensitivity to initial conditions makes it impossible to generate the surface in this

manner. In order to produce the complete surface, we will need to locate the curve which spawns them and use points along it to start subsequent integrations.

4. Conclusions

By reducing the original vector field to a set of critical points and their connections, we have arrived at a representation of the topology of a two-dimensional vector field, which is much smaller than the original data set but retains with full precision the information pertinent to the flow topology. This representation can be displayed as a set of points and tangent curves or as a graph, which is especially useful for comparing data sets and detecting topological transitions. When time defines a third dimension, the representation can be readily displayed as surfaces.

The two-dimensional analysis can be applied to the tangential velocity field near the walls of bodies to generate a skeleton of the surface topology. This skeleton can then be used to supply starting points for integrations and produce stream surfaces representing the surfaces of separation and the associated vortices.

Our work on developing methods for constructing representations of the topology of three-dimensional separated flows is still in progress. In addition to the separation topology, a three-dimensional flow may contain points in the volume where the magnitude of the velocity vanishes. These three-dimensional critical points can be classified [10] by a method analogous to the two-dimensional classification shown in Figure 1. Some classes of three-dimensional critical points have associated stream surfaces which need to be included to form a complete representation of the topology.

Eventually we hope to be able to fully characterize the topology and to generate surface representations of the complex structures as complete and informative as the hand drawn figures but supported by the quantitative information contained in the representation.

5. Acknowledgements

We wish to thank Brian Cantwell of Stanford, Stuart Rogers and Lewis Schiff of NASA Ames for providing us with interesting data sets.

This work is supported by NASA under contract NAG-2-489-S1, including support from the NASA Ames Numerical Aerodynamics Simulation Program and the NASA Ames Fluid Dynamics Division. The computing and graphics facilities are partially supported by the NSF under grant NCS 8815815.

References

[1] P. Buning and J. Steger. Graphics and flow visualization in computational fluid dynamics. In *Proceedings of the AIAA 7th Computational Fluid Dynamics Conference*, American Institute of Aeronautics and Astronautics, June 1985. Paper 85-1507-CP.

[2] M. Tobak and D. J. Peake. Topology of three-dimensional separated flows. *Annual Review of Fluid Mechanics*, 14:61–85, 1982.

[3] U. Dallmann. *Topological Structures of Three-Dimensional Flow Separation.* Technical Report DFVLR-IB 221-82 A 07, Deutsche Forschungs- und Versuchsanstalt für Luft- und Raumfahrt, April 1983.

[4] A. E. Perry and M. S. Chong. *Annual Review of Fluid Mechanics*, chapter A description of eddying motions and flow patterns using critical point concepts, pages 125–156. Annual Reviews Inc., 1987.

[5] J. L. Helman and L. Hesselink. Automated analysis of fluid flow topology. In *Three-Dimensional Visualization and Display Technologies*, SPIE Proceedings Vol. 1083, January 1989. Paper 1083-23.

[6] J. L. Helman and L. Hesselink. Representation and display of vector field topology in fluid flow data sets. *IEEE Computer*, 27–36, August 1989. Also appears in *Visualization in Scientific Computing*, G. M. Nielson & B. Shriver, eds. Companion videotape available from IEEE Computer Society Press.

[7] S. Rogers and D. Kwak. An upwind differencing scheme for time accurate incompressible navier-stokes equations. In *Proceedings of the AIAA 6th Applied Aerodynamics Conference*, American Institute of Aeronautics and Astronautics, June 1988. Paper 88-2583.

[8] S. X. Ying, L. B. Schiff, and J. L. Steger. A numerical study of three-dimensional separated flow past a hemisphere cylinder. In *Proceedings of the AIAA 19th Fluid Dynamics, Plasma Dynamics and Lasers Conference*, American Institute of Aeronautics and Astronautics, June 1987. Paper 87-1207.

[9] H. Fuchs, Z. M. Kedem, and S. P. Uselton. Optimal surface reconstructions from planar contours. *Communications of the ACM*, 20(10):693–702, October 1977.

[10] M. S. Chong, A. E. Perry, and B. J. Cantwell. A general classification of three-dimensional flow fields. *Physics of Fluids A*, 2(5):765–777, May 1990.